NeTrainSim: A Network Freight Train Simulator for Estimating Energy/Fuel Consumption

Ahmed Aredah
Center for Sustainable Mobility
Virginia Tech, Blacksburg, Virginia, USA, 24060
Email: AhmedAredah@vt.edu
ORCiD : https://orcid.org/0000-0003-0186-3783

Karim Fadhloun
Center for Sustainable Mobility
Virginia Tech, Blacksburg, Virginia, USA, 24060
Email: Karim198@vt.edu

Hesham Rakha
Director of Center for Sustainable Mobility
Virginia Tech, Blacksburg, Virginia, USA, 24060
Email: Hrakha@vt.edu
ORCiD: https://orcid.org/0000-0002-5845-2929

George List
Professor of Railway Engineering
North Carolina State University, Raleigh, North Carolina, USA, 27695
Email: gflist@ncsu.edu

Word Count: 6763 words + 3 tables (250 words per table) = 7444 words

Submitted 1/27/2023

ABSTRACT

Although train simulation research is vast, most available network simulators do not track the instantaneous movements and interactions of multiple trains for the computation of energy/fuel consumption. In this paper, we introduce the NeTrainSim simulator for heavy long-haul freight trains on a network of multiple intersecting tracks. Trains are modeled as a series of moving mass points (each car/locomotive is modeled as a point mass) while ensuring safe following distances between them. The simulator considers the motion of the train as a whole and neglects the relative movements between the train cars/locomotives. Furthermore, the powers of the different locomotives are transferred to the first locomotive as such a simplification results in a reduced simulation time without impacting the accuracy of energy consumption estimates. While the different tractive forces are combined, the resistive forces are calculated at their corresponding locations. The output files of the simulator contain information pertaining to the train trajectories and the instantaneous energy consumption levels. A summary file is also provided with the total energy consumed for the full trip and the entire network of trains. Two case studies were conducted to demonstrate the performance of the simulator. The first case study validates the model by comparing the output of NeTrainSim to empirical trajectory data using a basic single-train network. The results confirm that the simulated trajectory is precise enough to estimate the electric energy consumption of the train. The second case study demonstrates the train-following model considering six trains following each other. The results showcase the model's ability in relation to maintaining safe-following distances between successive trains. Finally, the NeTrainSim is demonstrated to be scalable with computational times in $O(n)$ for less than 50 trains and $O(n^2)$ for a higher number of trains (n).

Keywords: NeTrainSim, Network Trains Simulation, Energy Consumption

INTRODUCTION

The transportation sector is the largest consumer of total energy accounting for 26% of the US energy use in 2020 (*1*). With a cost reduction of about 75% when compared to other ground transportation modes, railroads account for roughly 40% of long-distance freight volume (*2*). The energy consumption of trains is influenced by various factors, including logistical, technical, and operational factors. Logistical factors are related to the trainload and network characteristics. Technical factors include vehicle physical characteristics such as the fuel type and aerodynamic parameters. Finally, operational factors include speed and driving dynamics (*3*).

The purpose of this paper is to describe an open-source Python simulator for heavy long-haul freight trains on a network where they interact with each other while producing valid instantaneous energy consumption estimates. The simulator, named NeTrainSim (Network Train Simulator), has been built specifically for energy consumption prediction of trains considering the main logistical, technical, and operational factors impacting them. Each car or locomotive in the train is considered a point mass positioned at the vehicle's center of gravity with only a longitudinal degree of freedom while ignoring lateral and vertical dynamics. The reason behind limiting the degree of freedom to the longitudinal component is justified by an expectation of a significant reduction in the computational simulation time.

The resistance forces, consisting of the aerodynamics, rolling, curve, and grade resistance, corresponding to each locomotive and car in the train are modeled at their specific location on the track. Furthermore, the simulator takes into account additional inputs for the mathematical representation of the train dynamics such as the network structure, track characteristics, and train parameters. NeTrainSim allows locomotives to be distributed along the train length in three locations: the head, the middle, and the end of the train. The distribution of cars with custom loads can easily be modified. NeTrainSim also includes a graphical user interface to facilitate the user's experience.

This research paper is structured as follows: First, an overview of the train dynamics model is presented. Then, a brief description of the NeTrainSim simulator is provided. Lastly, example case studies of two routes are presented to illustrate the simulator's performance.

LITERATURE REVIEW

While train simulation research is widespread, most existing simulators are unable to model the instantaneous train movements at scale. Specifically, multiple train simulators typically ignore the instantaneous motion of the train in order to achieve scalability. Alternatively, detailed train simulators are developed to simulate Longitudinal Train Dynamics (LTD) considering the motion of the train as a whole and/or any relative motion between vehicles in the direction of the train movement (*4*). Simulators found in the literature are of two types: whole-trip simulators and sectional or short-trip simulators.

As summarized in (*5*), whole-trip LTD simulators (*6*, *7*) replicate one fixed-configuration train running on a fixed route. Whole-trip simulators such as those developed by (*8*, *9*) are focused on calculating the in-train forces and their patterns with the vehicle connection system and draft gear behavior taken into consideration on a single track. Similarly, (*10*) provided a positioner model that optimizes the speed of the train to protect wagons from damage. According to (*5*), a drawback of these simulators is related to their lengthy simulation time due to the complexity of the involved models and computing strategies. The complexity of these models comes from the numerical solvers of differential equations — such as Runge-Kutta (*11*, *12*), Park Method (*13*), and others — that have been incorporated into these simulators.

A short-trip simulator has the same limitations as whole-trip simulators. Yet, they run relatively fast compared to their counterparts. While whole-trip simulators provide a more detailed assessment, short-trip simulators provide a microanalysis of a single train vehicle or the train as a whole (*14*). Other researchers proposed discrete mathematical models for the simulation of specific train systems. (*13*) provided a predictive model for couplers' forces in train cars due to electrodynamic braking. (*15*) developed a different type of simulation; their model optimized the train trajectory, number of vehicles, and hauled weights based on the track profile. Finally, (*16*) developed a simulator to predict pressure values in the air brake system.

Another simulator type is the one that was developed by the Federal Railroad Administration (FRA). The FRA-sponsored simulator is the Train Energy and Dynamics Simulator (TEDS). TEDS was developed for multiple purposes including conducting safety and risk evaluations, energy consumption studies, incident investigations, train operation studies, and ride quality evaluations. TEDS simulates the behavior of the train along the centerline of an ideal track with one degree of freedom (longitudinal motion) while discarding the vertical and lateral motion (*17*). Despite the robustness of the simulator, it only simulates one train on a single track.

The FRA sponsored another simulator named (ATTIF) to perform accident investigation, train configuration evaluation, and assist in the training of train operators. The ATTIF simulator uses simplified nonlinear dynamics of railroad vehicles that allow for maintaining a fair degree of accuracy and a relatively short simulation time (*18*). According to (*19*), ATTIF integrated a detailed multi-body dynamics coupler system model starting in 2012. In addition, the Train Dynamics and Energy Analyzer/train Simulator (TDEAS) was developed by the Chinese State Key Laboratory of Traction Power to perform detailed whole-trip longitudinal train dynamics and energy analyses (*7*). (*19*) summarize other simulators of friction draft gear modeling. Nevertheless, none of these simulators consider train energy consumption with respect to train forces and terrain topology.

Lastly, Cipek et al. (*20*)convert and simulate a conventional 103-ton and 1.6-MW heavy-haul diesel-electric locomotive to a battery hybrid equivalent and derive fuel consumption and related greenhouse gas emissions models. The results of this research are an accurate representation of train fuel and energy consumption. However, as concluded, the model cannot be generalized but could be considered as a basis for later studies.

MATHEMATICAL MODEL

The proposed train dynamics model is developed based on the 1992 Canadian National variation for resistance forces cited in (*21*) and refers to the models proposed in (*22*, *23*) for a tractive force and train-following model. TABLE 1 shows the model variable definitions.

TABLE 1 Model Variables Definition

Variable	Definition
$a_n(t)$	Acceleration of train n at instant t (m/s^2)
$\tilde{a}_n(t)$	Smoothed acceleration of train n at instant t (m/s^2)
$F_n(t)$	Tractive force of train n at instant t (N)
$R_n(t)$	Resistive force of train n at instant t (N)
$u_d(t)$	Desired speed or max speed a train can go by at instant t (m/s)
$u_n(t)$	Speed of train n at instant t (m/s)
$u_m(t)$	Train speed at maximum throttle at instant t (m/s)
$x_n(t)$	Position of the back of train n relative to the start of the trip (m)
$s_n(t)$	Spacing from rear bumper of train n to the rear bumper of train $n-1$ and is computed as $x_{n-1}(t) - x_n(t)$ (m)
T_n	The time it takes to activate the brakes of the train plus the operator perception reaction time (s)
t_1, t_2, t_3	Calibration parameters for throttle level
Δt	The solution time step (s)
s_n^j	Train spacing at jam density (m). Equal to the length of train n plus a buffer (taken to be 2m)
N	Notch Number
N_{max}	Number of Notches in the given locomotive
m_l	Total mass of locomotive l (kg)
m_c	Total mass of car c (kg)
m_l^a	Mass on single axle of locomotive l (kg)
m_c^a	Mass on single axle of car c (kg)
m	Train total mass $m = \sum_{c,l} m_{c,l}$ (sum of locomotive and car masses) (kg)
η	Mechanical efficiency of the transmission and gear
$\lambda_n(t)$	Throttle level of train n at instant t ($0 \le \lambda \le 1$)
λ^*	Throttle level that equates resistance forces at instance t ($0 \le \lambda \le 1$)
P_l^{max}	Maximum engine power of locomotive l (kW)
μ	Coefficient of friction between the wheel and the track
g	Gravitational acceleration (9.8066 m/s^2)
$K_{c,l}$	Canadian National streamlining coefficient of car c or locomotive l
A_l	Frontal area of locomotive l (m^2)
A_c	Frontal area of car c (m^2)
$G_{c,l}$	Track gradient of car c or locomotive l (%)
$C_{c,l}$	Track curvature of car c or locomotive l (degrees)
u_f	Track free-flow velocity (km/h)
$G(t)$	Grade of track at instant t (percent)
$\|\|c + l\|\|$	Number of cars and locomotives

Wang-Fadhloun-Rakha Throttle Forces

The dynamics model proposed in (*23*) is based on a prior one developed by (*22*). In both models, the throttle position is assumed to be hyperbolically proportional to vehicle speed. The throttle level increases up to a maximum with increasing speed and decreases when the speed approaches the desired speed (*23*). Equation (1) demonstrates the proposed hyperbolic throttle function.

$$\lambda_n(t) = \begin{cases} \dfrac{\dfrac{u_n(t)}{u_d(t)}}{t_1 + \dfrac{t_2}{1-\dfrac{u_n(t)}{u_d(t)}} + t_3\dfrac{u_n(t)}{u_d(t)}} & ,0 \leqslant u_n(t) \leqslant u_m(t) \\ \max\left(\dfrac{\dfrac{u_n(t)}{u_d(t)}}{t_1 + \dfrac{t_2}{1-\dfrac{u_n(t)}{u_d(t)}} + t_3\dfrac{u_n(t)}{u_d(t)}}, \lambda^*\right) & ,u_m(t) < u_n(t) \leqslant u_d(t) \end{cases} \quad (1)$$

Where variables t_1, t_2 & t_3 are calibrated parameters that were originally introduced in (*22*). These parameters are calculated based on the fact that the full capability of the vehicle motor power is never used and only around 60% of the vehicle capacity is used. However, in trains, this does not apply. Accordingly, these parameters are calibrated to reflect full usage of the train power as proposed in the (*23*) model. (*23*) proposed using 0.190, 0.152, and 0.050 for t_1, t_2, and t_3. However, these values were obtained for passenger trains and freight trains use more aggressive throttle levels. Thus, these values were adjusted to be 0.001, 0.050, and 0.030 respectively. It should be noted that the user can alter these default values as needed.

λ^* is the minimum throttle that is allowed to overcome resistance when the desired speed is reached. Equation (2) is used to calculate the λ^* that allows the vehicle to remain at the desired speed.

$$\frac{\min\left(\dfrac{1000\eta_n\lambda_n(t)P_l^{max}}{u_n(t)}, \mu m_l g\right) - R(u_d)}{M} = 0 \quad (2)$$

Unlike motor vehicles controlled by continuous throttle behavior functions, trains are controlled by discrete throttle notches, which results in incremental changes in throttle with running speed (*23*). Accordingly, the continuous function in Equation (1) is not to be directly applied to the train throttle forces without discretizing it first. To discretize the function (1), $\left(\frac{N}{N_{max}}\right)^2$ is used the approach described in (*4*). The rest of the procedure is addressed in (*23*).

NeTrainSim uses Equation (1) to calculate the throttle level based on the desired speed. The desired speed is a variable set to the maximum speed the locomotive can theoretically achieve. This variable value within the simulation framework is user-specified, however, based on a comprehensive review of relevant literature, a default value of 120 km/h was selected. Figure 1-left shows the discretized throttle level based on eight train notches and desired speed. The resulting discretization is aligned with the train number of notches in TABLE 2. The throttle level is then used to calculate the train tractive forces. Figure 1-right shows the tractive forces at different notches.

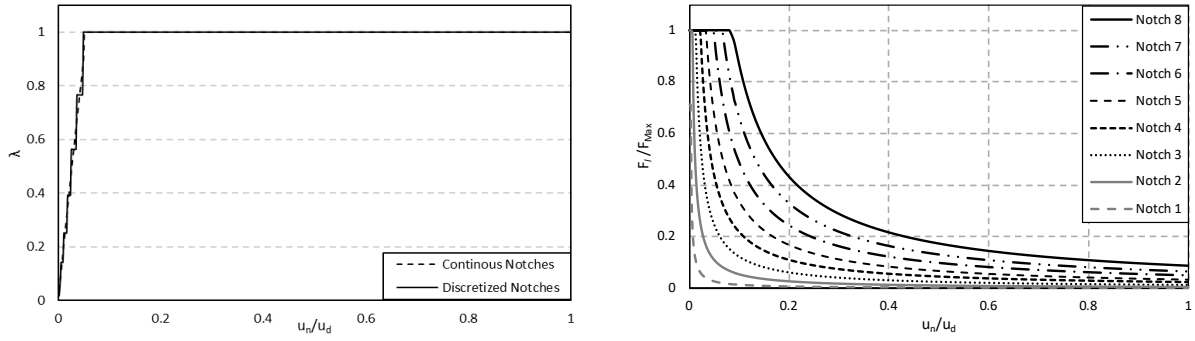

Figure 1 Throttle/notch level (left) and tractive force (right)

The net tractive force after overcoming the resistance forces is available to accelerate the train forward. The resistance forces change instantaneously on the track for each locomotive/car based on their attributes and location on the track. When the tractive forces are equal to the resistance forces, the train is unable to accelerate and travels at a constant speed. Alternatively, when the resistance force is higher than the tractive force, the train decelerates.

Hay Brake Force

(*4*, *24*) studied the brake forces of trains and concluded that the brake force is a piecewise function of train speed. With increasing speed, the brake force rises to its maximum retardation and is limited to a stable force level within a defined speed range. It then decreases at high speeds. In our model, we assume a constant desired deceleration level.

Canadian National Variation

The modified Davis Equation coefficients have been updated to reflect modern trains as demonstrated in Equation (3).

$$R_r = 1.5 + \frac{18N}{m_{l,c}} + 0.03u_n(t) + \frac{k_{c,l}A_{c,l}u_n^2}{10{,}000m_{l,c}} \quad (3)$$

Longitudinal Motion Model

The tractive force on each locomotive is computed using Equation (4). The model includes the basic tractive forces and the maximum force that can be sustained between the locomotive wheels and the track and includes a throttle function, as proposed by (*22*). The throttle function is discretized as described previously. The max train acceleration $a_n^{max}(t)$ is computed using Equation (5) as the difference between the total tractive force $F_n(t)$ and the total resistance forces $R_n(t)$ relative to the total mass m_n. The total tractive force is computed as the summation of the tractive forces on all the locomotives (l) using Equation (4). The throttle input used in Equation (4) is assumed to be the same for all locomotives.

$$F_{t|n}(t) = \sum_l \min\left(\frac{1000\eta_n\lambda_n(t)P_l^{max}}{u_n(t)}, \mu m_l g\right) \quad (4)$$

$$a_n^{max}(t) = \frac{F_n(t) - R_n(t)}{m_n} \quad (5)$$

Here a_n^{max} is train *n* maximum acceleration in m/s^2 at instant *t*, $F_{t|n}(t)$ & $R_n(t)$ are the train tractive and resistance forces in Newtons at instant *t*, m_n is train total mass in kg, η_n is train mechanical efficiency of the transmission and gear ($0 \le \eta \le 1$), P_l^{max} is the maximum locomotive engine power of train n in kW, $u_n(t)$ is velocity of train n at instant t in m/s, μ is coefficient of friction between the wheel and the track, m_l is total weight of locomotives in kg, and g is gravitational acceleration (9.8066 m/s^2).

The resistance forces are computed using the Canadian National variation of the Davis equation for both the locomotives and rail cars as in Equation (3). The gradient resistance force is added. Curve resistance is converted to an equivalent grade resistance by assuming that the unit resistance of a 1° curve is the same as the resistance of a 0.04% grade (*24*).

Hence the final resistance for each locomotive (l) or car (c) is $1.5 + \frac{18N}{W} + 0.03u_n + \frac{K_{c,l}A_{l,c}u_n^2}{10000W} + 20\left(G_{c,l}(t) + 0.04\left|C_{c,l}(t)\right|\right)$. Given that the Davis equation generates the resistance force in lbs., the unit

conversion (4.4482) is necessary to convert from units of lbs to Newtons. Equation (6) is the result of this conversion.

$$R_r = \frac{4.44822 \times 1.10231}{1000} \sum_{c,l} m_{c,l} \left(1.5 + \frac{16329.34}{m_{c,l}^a} + 0.0671 u_n(t) + \frac{48862.37 A_{c,l} K_{c,l} u_n(t)^2}{m_{c,l}} + 20\left(G_{c,l}(t) + 0.04\left|C_{c,l}(t)\right|\right) \right) \quad (6)$$

The modeling of train deceleration considers a constant deceleration d_{des}, which is user-specified but typically set at 0.2 m/s^2. We use a simple linear train-following model to compute the safe spacing between trains at steady-state conditions, s using Equation (7).

$$s_n(t) = s_n^j + T_n \, u_n(t) \quad (7)$$

Here, s^j is the spacing when stopped, which is taken to be the length of the train plus a buffer of 2m; T_n is the time it takes to activate the brakes plus the operator perception reaction time, t_{pr} and $u_n(t)$ is the velocity. T_n is estimated using Equation (8).

$$T_n = \frac{L_c^{max}}{u_s} + t_{pr} \quad (8)$$

Where L_c^{max} is the longest distance the brake signal needs to travel from the controlling locomotive to the last car in the batch of cars that are controlled by that set of locomotives. The brake signal is assumed to travel at the speed of sound (u_s) which is taken to be 343 m/s. t_{pr} is the operator perception reaction time (taken to be 4.5s in this paper as an average of what was found in (*25*) but can be user-specified). Using Equation (7), the terms are re-arranged to estimate the train following speed the next time step based on current spacing, as demonstrated in Equation (9).

$$\tilde{u}_n(t + \Delta t) = \min\left(\frac{s_n(t) - s_n^j}{T_n}, u_f \right) \quad (9)$$

Here u_f is the free-flow velocity of the track ahead of the train. The time-to-collision (TTC) is computed assuming the train continues at its current speed, as shown in Equation (10).

$$TTC = \min\left(\frac{s_n(t) - s_n^j}{\max(u_n(t) - u_{n-1}(t), 0.0001)}, TTC_{max} \right) \quad (10)$$

The desired acceleration, at some time into the future using the spacing at time t and incorporating it in the range policy presented in Equation (9), is computed twice. First assuming the speed is achieved over a time interval TTC (Equation 11) and the second is assumed to occur over a time interval T_n (Equation 12).

$$a_{n,1-1}(t) = \max\left(\frac{\tilde{u}_n(t + \Delta t) - u_n(t)}{TTC}, -\mu g \right) \quad (11)$$

$$a_{n,1-2}(t) = \min\left(\frac{\tilde{u}_n(t + \Delta t) - u_n(t)}{T_n}, a_n^{max}(t) \right) \quad (12)$$

We then compute the train acceleration as a weighted combination of the two accelerations, where the term β_1 is computed using Equation (14). The coefficient β_1 is a binary variable that is equal to zero when the acceleration is negative and equals one when the acceleration is either zero or positive. The first acceleration term is used for the train's negative accelerations (decelerations) while the second term is used for positive accelerations.

$$a_{n,1-3}(t) = (1 - \beta_1) a_{n,1-1}(t) + \beta_1 a_{n,1-2}(t) \quad (13)$$

$$\beta_1 = \frac{a_{n,1-1}(t) + |a_{n,1-1}(t)|}{2 \times \max(|a_{n,1-1}(t)|, 0.0001)} \quad (14)$$

An alternate train acceleration is computed by taking the Lagrangian derivative (a vehicle-based derivative) of Equation (9), as formulated in Equation (15).

$$a_{n,1-4}(t) = \max\left(\min\left(\frac{u_{n-1}(t) - u_n(t)}{T_n}, a_n^{max}(t)\right), -\mu g\right) \quad (15)$$

We then compute the train acceleration as a weighted combination of these two accelerations, where the term β_2 varies in the range [0,1]. The first acceleration term ($a_{n,1-3}(t)$) ensures that the train spacing between it and the train ahead complies with the range policy presented in Equation (9). The second acceleration term ($a_{n,1-4}(t)$) ensures that the train adjusts its speed to the speed of the train directly ahead.

$$a_{n,1}(t) = \beta_2 a_{n,1-3}(t) + (1 - \beta_2) a_{n,1-4}(t) \quad (16)$$

The complete train longitudinal motion model is a modification of the Fadhloun-Rakha car-following model (*22*) that is formulated in Equation (17). The first term computes the train acceleration when the speed of the train ahead of it is greater than or equal to its speed while the second term computes the train acceleration while approaching a slower-moving train. It ensures that the train attempts to decelerate at the desired deceleration level (d_{des}).

$$a_n(t) = (1 - \gamma) a_{n,1}(t) - \gamma a_{n,2}(t) \quad (17)$$

The other parameters are computed as:

$$a_{n,2}(t) = \min\left(\frac{(u_n(t)^2 - u_{n-1}(t)^2)^2}{4\left(\max\left(s_n(t) - s_n^j - T_n u_n(t), 0.0001\right)\right)^2 d_{des}}, \mu g\right) \quad (18)$$

$$\gamma = \frac{u_n(t) - u_{n-1}(t) + \sqrt{\left(u_n(t) - u_{n-1}(t)\right)^2}}{2 \times \max(|u_n(t) - u_{n-1}(t)|, 0.0001)} \quad (19)$$

When the train spacing is greater than s_{lad}, the movement of the train is assumed to be free of train interaction and is achieved using $a_n^{max}(t)$.

$$s_{lad} = s_{j_n - 1} + T_n u_f + \frac{u_f^2}{2 \times d_{des}} \quad (20)$$

The acceleration is constrained by the maximum jerk allowed (j_{max}), as shown in Equation (21).

$$a_n(t) = \min(|a_n(t)|, |a_n(t - \Delta t) + j_{max} \Delta t|) \cdot (-1)^p \quad , p = \begin{cases} 0, & a_n(t) \geq 0 \\ 1, & a_n(t) < 0 \end{cases} \quad (21)$$

The smoothed acceleration $\tilde{a}_n(t)$ is then computed using an exponential smoother, as demonstrated in Equation (22). Here α is the exponential smoother. A smoothing factor value of 1.0 provides no smoothing and lower values provide more smoothing.

$$\tilde{a}_n(t) = \alpha \times a_n(t) + (1 - \alpha) \times \tilde{a}_n(t) \quad (22)$$

The train speed is computed using the first-order Euler approximation, as formulated in Equation (23).

$$u_n(t + \Delta t) = \max\left(\min\left(u(t) + \tilde{a}(t) \times \Delta t, u_f\right), 0\right) \quad (23)$$

Energy Use Model

The energy use model is based on (*26*). The former was developed for a metro rail setting. It is true that auxiliary energy consumption is needed for specific commodities, but this energy use is ignored.

The power (instantaneous energy use) to move the train forward is computed using Equation (24).

$$P_{W|n}(t) = \left(m_n a_n(t) + R_n(t)\right) \times u_n(t) \tag{24}$$

Where the resistance forces $R_n(t)$ are estimated using equation (6) including the resistance that is being overcome. $m_n a_n(t)$ represents the net tractive forces the train is producing at every time step. A regenerative coefficient is used to estimate the portion of energy that can be regenerated due to deceleration. The energy regenerative coefficient $\eta_{re|n}$is a function of deceleration level as shown in Equation (25).

$$\eta_{re}(t) = \begin{cases} \dfrac{1}{e^{\frac{\alpha}{|a(t)|}}} & \forall\, P_{W|n}(t) < 0 \\ 0 & \forall\, P_{W|n}(t) \geqslant 0 \end{cases} \tag{25}$$

Equation (26) estimates the energy consumed by the train's tractive forces when it is consuming energy (when Power P_n is greater than zero). Conversely, when the train is braking (power is less than zero), the train can only recapture a fraction of the tractive power as shown in Equation (24) while the rest is dissipated in heat form.

$$P_{B,n}(t) = \begin{cases} \dfrac{P_{W|n}(t)}{\eta_{W-T}} + P_A, & \forall\, P_{W|n}(t) > 0 \\ P_{W|n}(t) \times \eta_{re|n} \times \eta_{W-T} + P_A & \forall\, P_{W|n}(t) \leq 0 \end{cases} \tag{26}$$

η_{W-T}, the train driveline efficiency is assumed to be a multiplicative combination of a wheel-to-DC bus efficiency and DC-bus-to-tank efficiency, as shown below. The DC bus is chosen as an intermediate node in the energy transfer process because it is used across multiple energy delivery technologies (e.g., diesel fuel, batteries, and hydrogen fuel cells). The DC bus-to-tank efficiency (η_{B-T}) is highly dependent on the locomotive energy source, as illustrated in Figure 2. The wheel-to-Bus efficiency (η_{W-B}), is an invariant relationship (for a given locomotive) and does not depend on the energy source. Rather, it depends on the train speed, and it is found to be steady at 90% after ~12.2 m/s (~43 km per hour). If the train has locomotives with a variety of energy sources, the above equations (24 and 26) are used for each locomotive.

$$\eta_{W-T} = \eta_{W-B} \times \eta_{B-T} \tag{27}$$

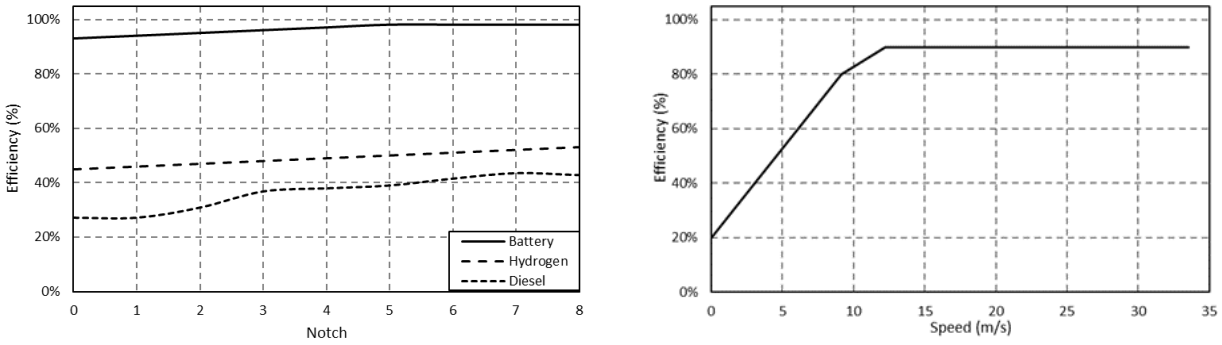

(A*) DC Bus to Tank Efficiency by Notch Number* *(B) Wheel to DC Bus Efficiency by train Speed*

Figure 2 Locomotives drive-line efficiencies by energy source

The energy consumed is calculated by multiplying the power in Equation (26) by the time step length. The product 1000×3600 is used to convert this value into Kilowatt-hours.

$$EC_n(t) = \frac{P_{B,n}(t)}{1000 \times 3600} \times \Delta t \tag{28}$$

Train Delay and Number of Stops Estimation

The train delay is computed at each time step for each locomotive/car by comparing its travel time to its travel time if driven at the free-flow speed of the corresponding track it is on, as shown in Equation (29). This is based on previous work done in the traffic domain and validated against (*27*). The delay for a specific train/trip is then computed as the summation of the delays across all the time steps that constitute the trip. The total network delay is then computed as the summation of the total delay of all trains simulated.

$$d_n(t) = \frac{\sum_{c,l}\left(1 - \frac{u_n(t)}{u_{f|c,l}}\right) \times \Delta t}{\|c + l\|} \tag{29}$$

Similarly, the number of stops the train incurs is computed based on work done in the traffic flow domain (*28*), as demonstrated in Equation (30). This equation captures all partial stops incurred by the train each time step and then is summed up across all time steps to compute the number of stops experienced by the train. This is then summed up across all the trains to compute the total number of stops incurred across the network of trains.

$$s_n(t) = \begin{cases} \frac{\sum_{c,l}\left(\frac{u_n(t-\Delta t) - u_n(t)}{u_{f|c,l}}\right)}{|c + l|} & u_n(t-\Delta t) > u_n(t) \\ 0 & \text{otherwise} \end{cases} \tag{30}$$

SIMULATOR DESCRIPTION

NeTrainSim is written using the Python scripting language with functional programming in mind, so it is maintainable and easy to read and debug. Since Python is a dynamic language and is not computationally fast when compared to other programming languages, "Cython" is used to convert it to C, which is much better in terms of computational speed. This code transformation is advantageous because it keeps the editing language as Python, which helps with readability.

NeTrainSim is able to simulate the behavior of multiple trains on a given network. The network is defined as a graph connecting nodes with links. The simulator also allows the implementation of signals at specified nodes. The simulator is a dynamics-based longitudinal motion simulator in that it allows the modeling of both tractive and resistive forces acting on the trains, while also incorporating train-following models that govern their behavior when in the vicinity of each other. The simulator is a time-driven algorithm that calculates the movements of the different trains at each time step of the simulation. Once completed, a summary file is generated containing information pertaining to the trains' travel time, traveled distance, consumed energy, and fuel consumption. The consumed energy model assumes that all the train locomotives are of the same type.

The simulator is divided into modules and each module handles a set of tasks. The network module handles the network calculations and defines the network structure. The train dynamics module defines the train characteristics, their paths, and their movement dynamics. The energy module handles energy consumption calculations with different energy sources. Lastly, the simulator module is the central component where all calculations are synchronized, and actual train movements are simulated.

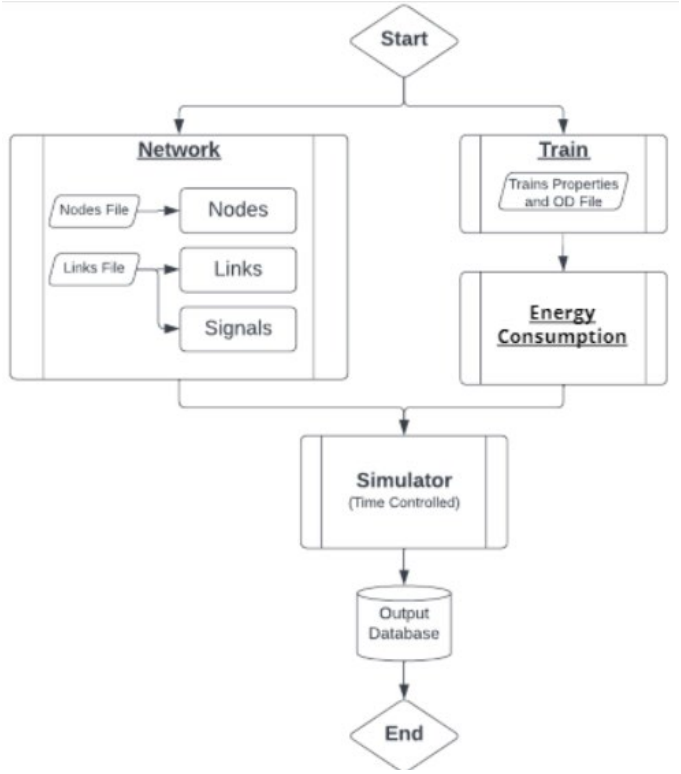

Figure 3 Simulator schema

The network links are assumed to be linear (only in length calculations). This is because the simulator uses vectors to calculate the trains' coordinates and reduce the calculation time. Vectorization requires the links to be linear instead of curves since curves are composed of millions of approximated vectors.

Line segments are treated as a piecewise sequence of links. Each link has a constant grade, curvature, and speed limit. When these links are short relative to the train length, the train spans many links. Therefore, every car or locomotive has its specific grade, curvature, and maximum allowed speed. The train is not allowed to exceed the maximum speed of any of the train-spanned links. Furthermore, trains must reduce their speed before entering a link that has a free-flow speed (speed limit) less than the train's current speed.

NeTrainSim (Figure 4) starts by setting the locations where the speed must be zero (e.g., for crew changes). If no stops are specified, which is the default, a stop is specified at the end of the route. The main driving point of the simulator is checking whether all trains reach their destination. The simulation ends when all trains have reached their destinations. A summary file is then generated along with an optional trajectory file. If at least one train does not reach its destination, the simulator first determines the trains for which the trip is still in progress and then runs the calculations specifically for those trains until they all reach their destinations.

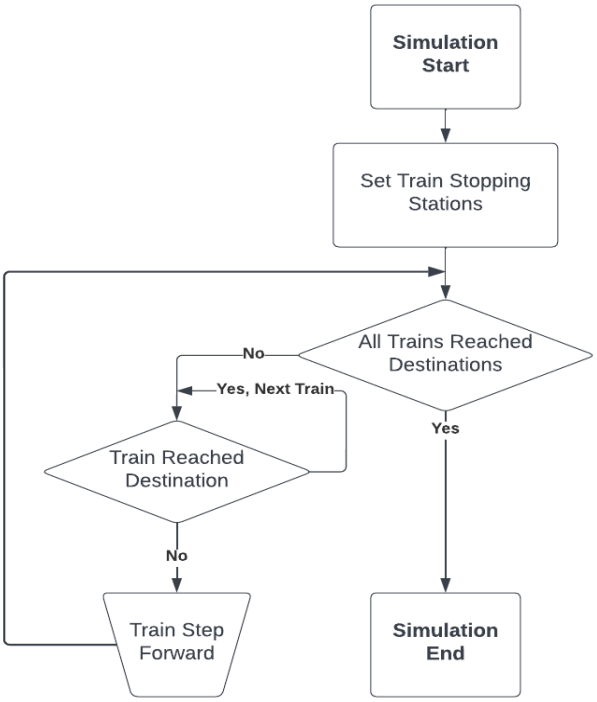

Figure 4 Simulation flow chart

At each time step (Figure 5), the simulator retrieves the grade, curvature, and free-flow speed for every unit in every train.

The simulator uses this information to calculate resistance forces. In addition, the simulator sets the maximum speed that each train can go based on the maximum allowable speed for all units in a given train. Simultaneously, the simulator calculates how far it is to the next stopping station, reduced-speed point, or train ahead. This ensures that the train reduces its speed appropriately without colliding with other trains.

All the gathered information is passed to the train dynamics module to calculate how much acceleration or deceleration is required. This speed is used to compute the incremental distance traveled during the current time step. This distance is added to the train's cumulative traveled distance. Lastly, the energy consumption of the train is calculated based on the train characteristics as stated in (*29*). All trains are advanced in the same manner.

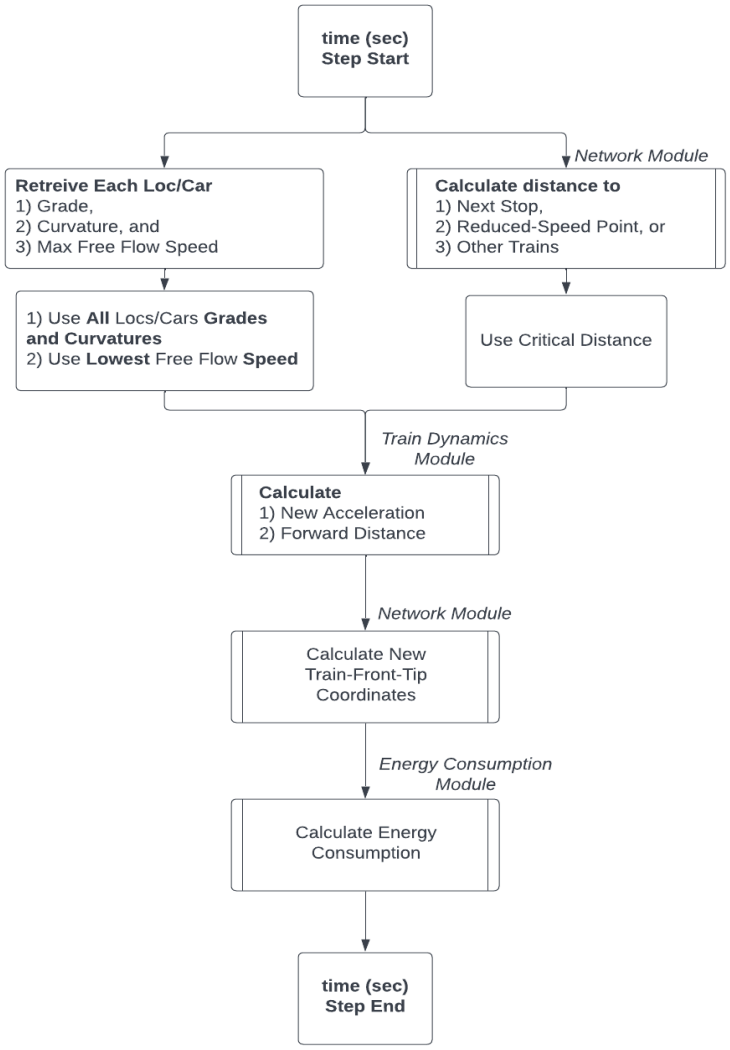

Figure 5 Time step simulation calculations

CASE STUDIES

Two scenarios are presented here (I and II), with train characteristics shown in TABLE 2. The first attempts to validate NeTrainSim against empirical train trajectory data. That is achieved by simulating the actual network on which the empirical trajectory was collected and setting the train characteristics similar to those of the train that completed the trip. The validation of the simulator can be, thus, achieved by comparing the simulated trajectory to the empirical field-based observations. The second scenario primarily demonstrates the performance of the train-following model implemented in the simulator in terms of regulating the longitudinal motion of the trains when following one another. In that regard, the second scenario involves six trains following each other. The second through sixth trains are shorter and lighter than the first, by 50% to ensure that they can catch up with the lead train.

Scenarios (*I*) and (*II*) are one-way tracks of lengths 162 and 322 km, respectively, with 4 intermediate stopping stations. These stations force the train to stop completely and then move again. The stops are distributed as shown in TABLE 2. The trains start and end their trips with a speed equal to zero. The tracks consist of 207 and 156 one-way links for scenarios (*I*) and (*II*), respectively, with lengths varying between 0.3 and 9 km. Different grade, curvature, and maximum speed combinations are assigned to every link along the track (as shown in Figure 6 and Figure 10).

TABLE 2 Trains Characteristics used in Scenario I (Left) and II (Right)

Train Characteristics	Value
Track Length (km)	162
Stopping Stations at (km)	40;42;88;150
Transmission Efficiency	0.98
Max Locomotive Power (kw)	3262
Number of Locomotives	3
Number of axles per Locomotive	6
Coefficient of Friction	0.25
First Locomotive K Value	24
Other Locomotives K Value	5.5
Cars k Value	5
Locomotives' Frontal Area (m^2)	14.8645
Cars Frontal Area (m^2)	12.0774
Number of Cars	71
Number of Car Axials	4
Locomotive Length (m)	22.3
Car length (m)	29
Locomotive Weight (ton)	198
Car Weight (ton)	44
Grade (%)	0~2.4
Curvature (%)	0

Train Characteristics	Value
Track Length (km)	322
Stopping Stations at (km)	40;42;88;150
Transmission Efficiency	0.82
Max Locomotive Power (kw)	2445.9
Number of Locomotives	11
Number of axles per Locomotive	6
Coefficient of Friction	0.25
First Locomotive K Value	24
Other Locomotives K Value	5.5
Cars k Value	5
Locomotives' Frontal Area (m^2)	14.8645
Cars Frontal Area (m^2)	11.1484
Number of Cars	139
Number of Car Axials	4
Locomotive Length (m)	23
Car length (m)	20.7
Locomotive Weight (ton)	190
Car Weight (ton)	100
Grade (%)	0~2
Curvature (%)	0~5

Scenario I

Figure 6 shows the train speed profile for the first scenario. The traveled distance is shown on the x-axis and the speed in m/s on the y-axis. The dotted line presents the field measurements. Note that at high-grade values (dashed line), the speed drops as the train decelerates as a result of the significant increase in the resistance forces. For instance, at a distance of 35 km (Figure 6-b), the speed drops from 25 to 22 m/s due to a grade of 2%.

The speed profile from the field data is provided for comparison with the model's results. The acceleration/deceleration decisions of the model logic are somewhat different from that of the train operator. In zone Figure 6-a, both our simulator and the driver showed similar behavior in accelerating; however, the operator is found to be less aggressive than our model prediction as described by Equation (1). Figure 6-c expressed a similar behavior except the driver is slightly more aggressive than in Figure 6-a. In Figure 6-b, both the driver and the simulator decreased their speed to accommodate the stopping station. Nevertheless, the simulator is found to be more forceful on the brakes than the driver. In Figure 6-d, the driver reduced his speed unlike what the simulator did.

Statistics results show that the simulated trajectory resulted in 10 minutes and 44 seconds of delay and 8.0 of stops for the leading train.

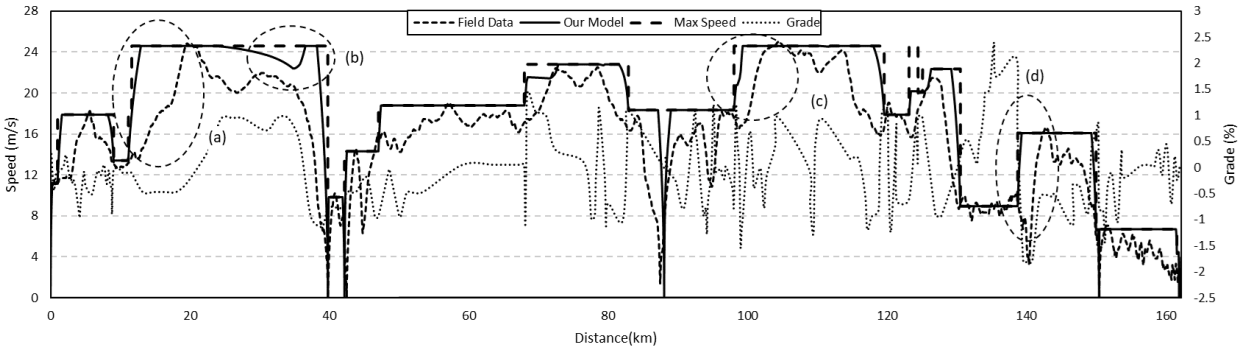

Figure 6 Speed profile of the train in scenario I

Figure 7 plots the simulated and empirical acceleration profiles as a function of the traveled distance. The figure shows that the operator continuously changes the train's speed and thus there is more noise in the empirical data. However, there are spots like those highlighted in Figure 7 where the acceleration decisions are similar.

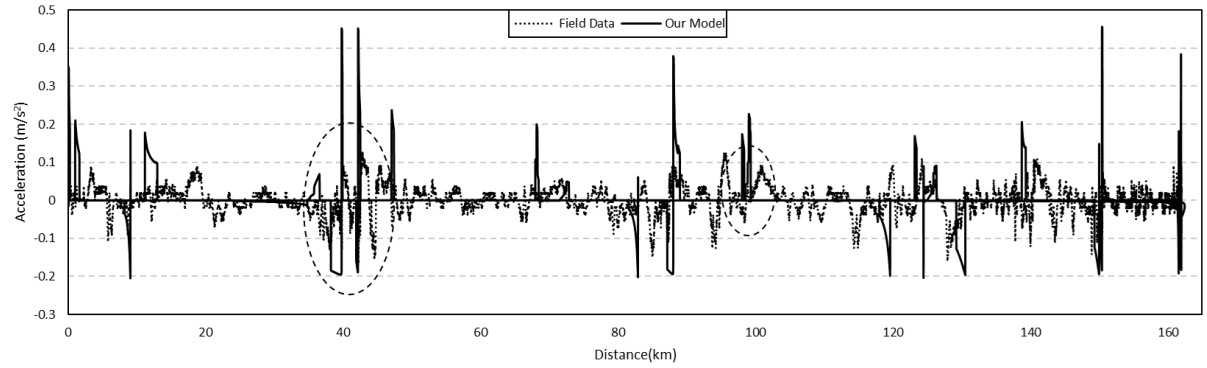

Figure 7 Acceleration profile of the train in scenario I

The acceleration provided in Figure 7 is the actual acceleration used to change the train speed. Another interesting acceleration profile refers to the one resulting from the application of the brakes to reduce the speed in order to not exceed the free-flow speed on a downgrade. This is another type of acceleration, referred to as virtual acceleration, which is used to regenerate energy, along with the observed deceleration, as indicated in Equation (28). Figure 8 shows this virtual acceleration profile. Figure 8-a is an instance of applying the brakes at a downgrade section while maintaining the train's speed.

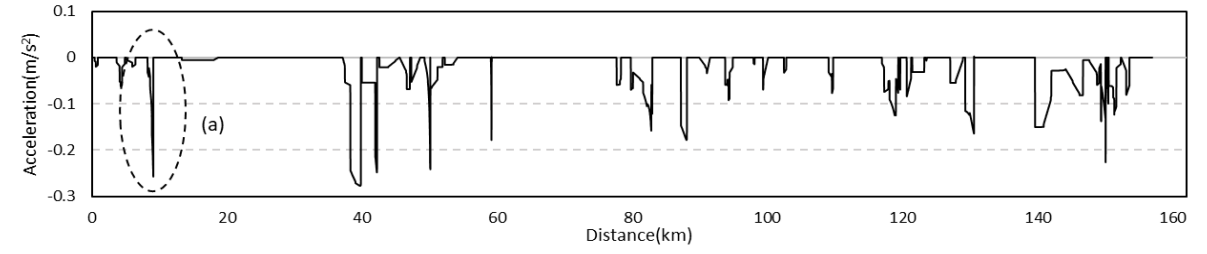

Figure 8 Virtual acceleration profile of the train in scenario I

Figure 9 shows the rate of Energy Consumption (EC) of the train. Equation (28) is used to calculate it. As shown, this rate is following the speed profile. The energy consumption rate is the highest when the train is accelerating from a speed of zero and is lowest when the train is decelerating. When the EC is below zero, this indicates the train is regenerating energy and storing it in its batteries. The model predicts the

total energy consumed to be 10.12 megawatt-hours while the field data show an energy consumption of 10.58 megawatt-hours, which corresponds to a 4.5 percent difference. In addition, if this train, with the same configuration and weights, was running on diesel, the energy consumption approximately increases by 150% (equal to 26.64 megawatt-hours or 761.36 diesel fuel gallons).

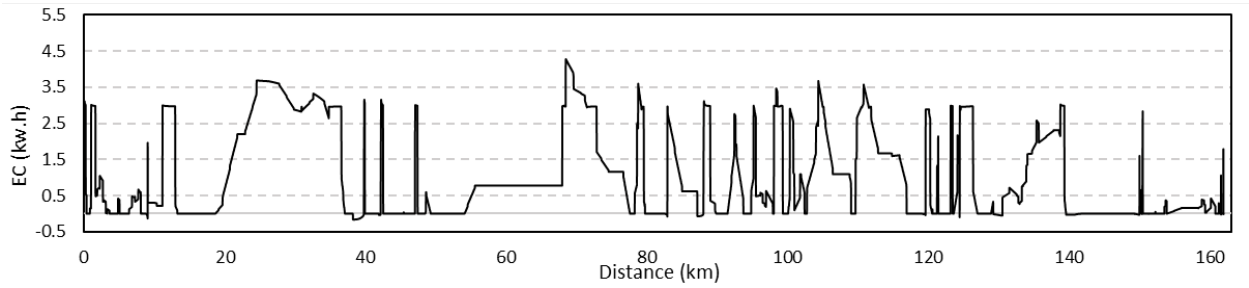

Figure 9 Energy consumption profile of the train in scenario I

Scenario II

Similarly to Scenario I, we start by presenting information pertaining to the leading train speed profile in Figure 10 as a function of the distance traveled (solid line). The dashed lines present the speed limit (also known as the free-flow speed) on each of the links along the train path. The profile shows, sections with high grades and decelerating speeds. For example, at a distance of approximately 14 km (Figure 10-a), the speed drops from 17 to 6 m/s due to an uphill grade of 2%.

There are also sudden drops in speed like the one at approximately 64 km (Figure 10-b) because of stops at stations. Also, the train does not exceed the speed limit of any link. Moreover, the train reduces its speed before leaving a high-speed link approaching a low-speed link as indicated at distance ~90 km in Figure 10-c. Statistics results show the simulated trajectory resulted in 1 hour and 20 minutes of delay and 11.8 of stops for the leading train.

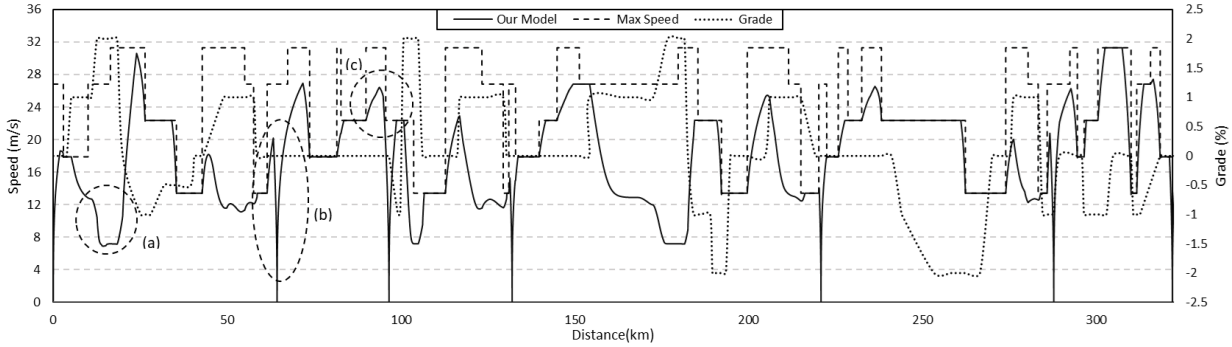

Figure 10 Speed profile of the leading train (train 1) in scenario II

The leading train's acceleration profile is shown in Figure 11. The maximum acceleration comes right after a complete stop, and it is relatively high when the train is increasing its speed. When the deceleration is constant, the jerk is near zero, due to the smoothing function in Equation (22) which constrains the train's ability to reach the maximum deceleration level as soon as the brakes are applied.

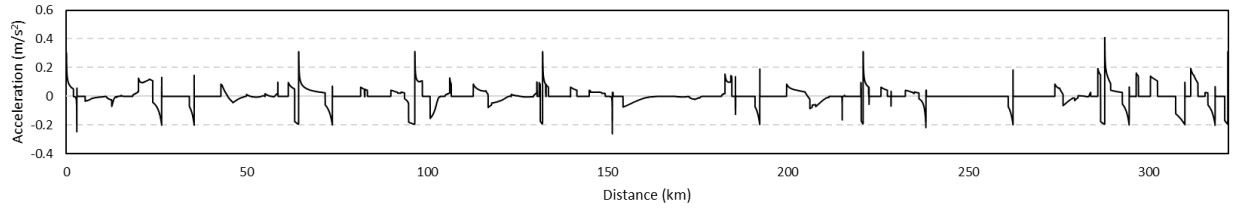

Figure 11 Acceleration profile of the leading train (train 1) in scenario II

Figure 12 shows the rate of energy consumption for the leading train in scenario II. The total energy consumed by the leading train is found to be 83.5 megawatt-hours. For the following trains, it is around 50.6 megawatt-hours. The same configuration of the leading train would consume 382 megawatt-hours with approximately 10,931 diesel gallons.

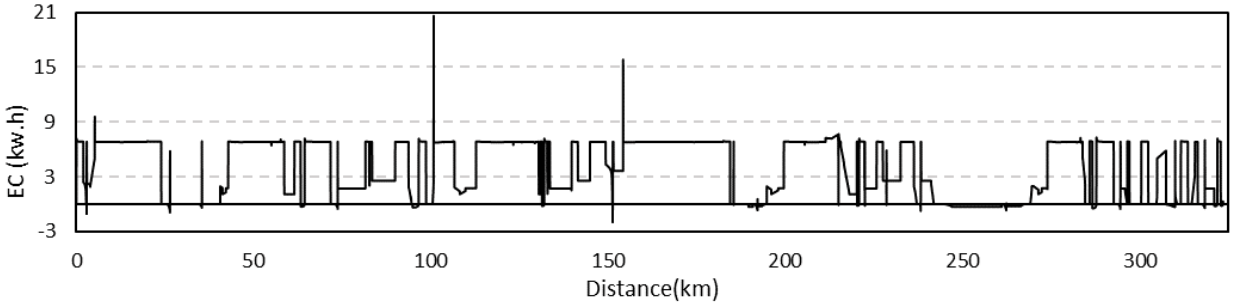

Figure 12 Energy consumption profile of the leading train (train 1) in scenario II

Figure 13 shows the time-space diagrams of the different trains. The slope of each train trajectory allows the determination of the instantaneous speed at a particular time. The first train (train 1) moves freely. Its speed is limited only by the maximum speed and its propulsive and braking capabilities. The speed reductions are due to these limitations. The following trains are constrained by the lead train. The initial headways are 1000 seconds to allow each train to traverse a significant distance before being impeded by the train ahead of it. At 14 and 170 km, the resistance forces are large due to high grades; and train 1 slows down. Trains 2-6 slow at that location and follow each other at the minimum allowable headway. At ~100km, train 1 reaccelerates and the headways increase again until ~200km.

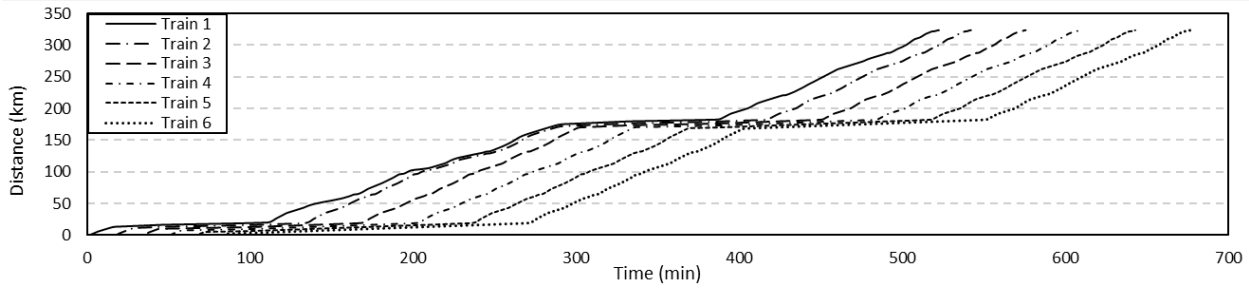

Figure 13 Scenario II trains' time-space diagram

Figure 14 shows the headways between trains. Since train 1 does not follow another train, its headway is not shown. As can be seen, the headway trends are similar for trains 2-6 but displaced in time. At the beginning of each train's trajectory, it travels at the maximum allowed speed until the headway is less than s_{lad} as calculated by Equation (20). At that point, the train reduces its speed to follow the train ahead. At approximately 600 minutes, train 1 reduces its speed because of the significant grade. The rest of the trains bunch up behind it as a consequence of their faster speeds. After this, train 1 reaccelerates and

the following trains move freely. Once each train reaches its destination, the plot of its headway to the train ahead ceases to be plotted.

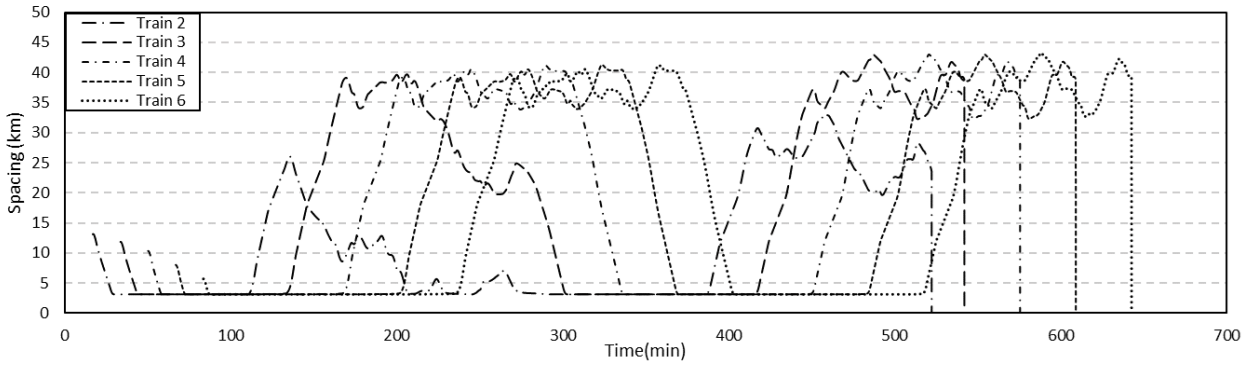

Figure 14 Scenario II trains' headway to leading train

Simulator Results Interpretation

The simulator uses discrete time steps to update the speeds, accelerations, energy consumption levels, and all the dependent statistics of the different trains. The smaller the step size is, the more accurate the results are. In TABLE 3, the model predictions for different time step sizes are compared for Scenarios I and II. As can be seen, using a time step of three seconds reduces the total simulation time by ~60% (relative to the 1-second time-step case) while the resultant statistics are largely unchanged. Increasing the time step beyond three seconds creates more significant changes in the predictions.

TABLE 3 Time step sensitivity analysis

Time Step (sec)	Sim Time (h:mm:ss)		Total EC (MWh)		Avg. Delay Time (h:mm:ss)		Avg. Stops	
	Scenario I	Scenario II	Scenario I	Scenario II	Scenario I	Scenario II	Scenario I	Scenario II
1 (Ref diff%)	0:00:15 (00%)	0:02:54 (00%)	10.12 (0.00%)	441.71 (0.00%)	0:10:44 (00%)	1:28:55 (00%)	8.0 (00.0%)	15.3 (00.0%)
2	0:00:08 (-33%)	0:01:35 (-46%)	10.12 (0.03%)	443.33 (0.37%)	0:11:07 (04%)	1:29:39 (01%)	8.0 (00.2%)	15.6 (02.0%)
3	0:00:06 (-61%)	0:01:05 (-63%)	10.18 (0.55%)	444.67 (0.67%)	0:11:37 (08%)	1:30:11 (01%)	8.0 (00.0%)	15.8 (03.4%)
4	0:00:05 (-68%)	0:00:51 (-71%)	10.14 (0.16%)	445.92 (0.95%)	0:12:08 (13%)	1:31:10 (03%)	8.2 (02.1%)	16.2 (06.0%)
5	0:00:04 (-71%)	0:00:43 (-76%)	10.22 (1.02%)	447.35 (1.28%)	0:11:39 (09%)	1:31:31 (03%)	8.1 (01.9%)	16.3 (07.0%)
6	0:00:03 (-74%)	0:00:35 (-80%)	10.27 (1.52%)	450.25 (1.93%)	0:12:21 (15%)	1:32:11 (04%)	8.1 (00.9%)	16.9 (10.5%)
7	0:00:03 (-80%)	0:00:33 (-81%)	10.21 (0.89%)	450.29 (1.94%)	0:12:42 (18%)	1:32:39 (04%)	8.0 (00.3%)	17.3 (13.3%)
8	0:00:03 (-84%)	0:00:27 (-85%)	10.23 (1.06%)	452.04 (2.34%)	0:12:18 (15%)	1:32:34 (04%)	8.1 (01.2%)	17.6 (15.7%)
9	0:00:02 (-84%)	0:00:23 (-87%)	10.24 (1.22%)	455.81 (3.19%)	0:12:02 (12%)	1:33:08 (05%)	7.6 (-04.9%)	17.4 (14.2%)
10	0:00:02 (-88%)	0:00:23 (-87%)	10.23 (1.14%)	457.02 (3.47%)	0:12:20 (15%)	1:32:29 (04%)	8.2 (02.1%)	18.0 (17.8%)

To test the simulator's scalability, multiple successive train cases (from one to 200 trains) were simulated using the network of Scenario II. The simulation time for the 200 trains case was 5 hours and 52 minutes. The tests were carried out on a laptop with an Intel® Processor Core i7-8750H and 32GB RAM. The growth function is linear up to 50 trains and quadratic after that.

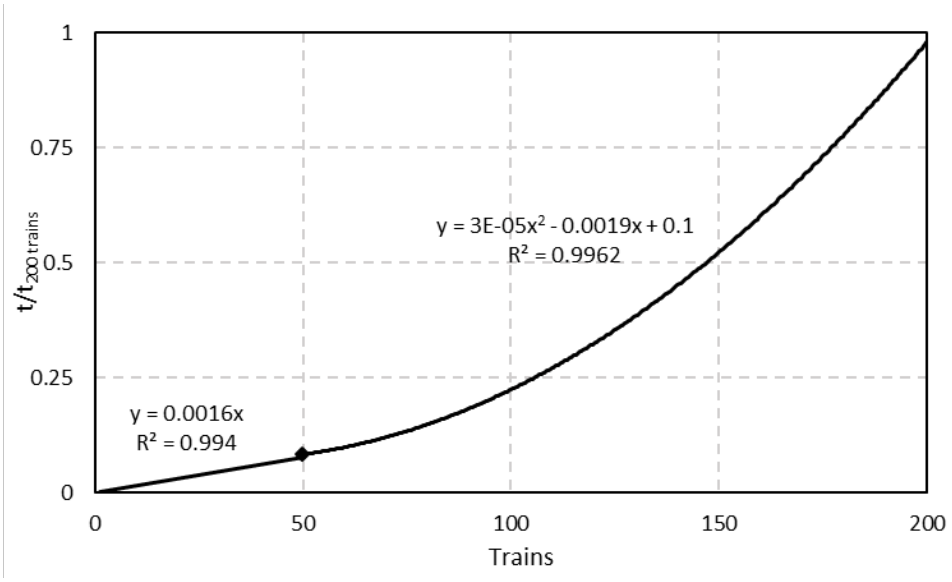

Figure 15 NeTrainSim scalability test

CONCLUSIONS

In this paper, we present NeTrainSim, a unique open-source multi-train simulator for fuel and energy prediction of diesel and electric freight trains. NeTrainSim is a dynamics-based simulator that uses train-following strategies adapted from traffic flow theory in combination with train dynamics modeling to control the longitudinal motion behavior of the different trains. Given that freight trains are very long, the model decomposes the train into its constituent locomotives and cars in computing the resistance forces on the train The simulator outputs consist of different metrics such as the instantaneous accelerations, speeds, positions, fuel/energy consumption levels, delays, and stops of all the trains in the simulated network. The tool is demonstrated to produce results similar to empirical data confirming that the model produces defensible results for travel times, speed trends, and energy consumption of the trains. As of now, the simulator does not capture the so-called energy consumption "at the well" or at the ultimate energy source. Nevertheless, the simulator can compare energy consumption characteristics for different energy technologies insofar as onboard energy use is concerned. The tool is demonstrated to be scalable with computational times in the $O(n^2)$, where n is the number of trains.

ACKNOWLEDGMENTS

This work was supported by the US Department of Energy.

AUTHOR CONTRIBUTIONS

The authors confirm their contribution to the paper as follows: study conception and design: Aredah, Rakha, and George; model reviewing: Fadhloun; analysis and interpretation of results: Aredah. All authors reviewed the results and approved the final version of the manuscript.

REFERENCES

1. U.S. Energy Information Administration. Annual Energy Outlook 2022. https://www.eia.gov/outlooks/aeo/data. Accessed May 19, 2022.
2. Association of American Railroads. *Freight Railroads & Climate Change*. 2021.
3. Ia-, A. G., and I. G. Alez-franco. Energy Consumption and Carbon Dioxide Emissions in Rail and Road Freight Transport in Spain : A Case Study of Car Carriers and Bulk. 2012.
4. Iwnicki, S., M. Spiryagin, C. Cole, and T. McSweeney, Eds. *Handbook of Railway Vehicle Dynamics*. CRC press, 2006.
5. Wu, Q. *Optimisations of Draft Gear Designs for Heavy Haul Trains*. Central Queensland University, Australia, 2017.
6. Cole, C. Longitudinal Train Dynamics: Characteristics, Modelling, Simulation and Neural Network Prediction for Central Queensland Coal Trains. 2017.
7. Wu, Q., S. Luo, and C. Cole. Longitudinal Dynamics and Energy Analysis for Heavy Haul Trains. *Journal of Modern Transportation*, Vol. 22, No. 3, 2014, pp. 127–136. https://doi.org/10.1007/s40534-014-0055-x.
8. Shabana, A. A., A. K. Aboubakr, and L. Ding. Use of the Non-Inertial Coordinates in the Analysis of Train Longitudinal Forces. *Journal of Computational and Nonlinear Dynamics*, Vol. 7, No. 1, 2012. https://doi.org/10.1115/1.4004122/465847.
9. Kovalev, R., A. Sakalo, V. Yazykov, A. Shamdani, R. Bowey, and C. Wakeling. Simulation of Longitudinal Dynamics of a Freight Train Operating through a Car Dumper. *Vehicle System Dynamics*, Vol. 54, No. 6, 2016, pp. 707–722. https://doi.org/10.1080/00423114.2016.1153115.
10. Qi, Z., Z. Huang, and X. Kong. Simulation of Longitudinal Dynamics of Long Freight Trains in Positioning Operations. *Vehicle System Dynamics*, Vol. 50, No. 9, 2012, pp. 1409–1433. https://doi.org/10.1080/00423114.2012.661063.
11. Chen, C., M. Han, and Y. Han. A Numerical Model for Railroad Freight Car-to-Car End Impact. *Discrete Dynamics in Nature and Society*, Vol. 2012, 2012.
12. Jin, X., and Y. Luo. The Mathematic Description of Features of the Friction Type Draft Gears. *Rolling Stock*, Vol. 49, No. 6, 2011, pp. 1–4.
13. Varazhun, I., A. Shimanovsky, and A. Zavarotny. Determination of Longitudinal Forces in the Cars Automatic Couplers at Train Electrodynamic Braking. *Procedia Engineering*, Vol. 134, 2016, pp. 415–421. https://doi.org/10.1016/j.proeng.2016.01.032.
14. Evans, J., and M. Berg. Challenges in Simulation of Rail Vehicle Dynamics. *Vehicle System Dynamics*, Vol. 47, No. 8, 2009, pp. 1023–1048. https://doi.org/10.1080/00423110903071674.
15. Li, W., S. Jiang, and M. Jin. Multi-Objective Optimization and Weight Selection Method for Heavy Haul Trains Trajectory. *IEEE Access*, 2022.
16. Wei, W., and Y. Lin. Simulation of a Freight Train Brake System with 120 Valves. *Proc Inst Mech F J Rail Rapid Transit*, Vol. 223, No. 1, 2009, pp. 85–92. https://doi.org/10.1243/09544097jrrt119.
17. Andersen, D. R., G. F. Booth, A. R. Vithani, S. P. Singh, A. Prabhakaran, M. F. Stewart, and S. K. (John) Punwani. Train Energy and Dynamics Simulator (TEDS): A State-of-the-Art Longitudinal Train Dynamics Simulator. 2012.
18. Sanborn, G. G., J. R. Heineman, and A. A. Shabana. A Low Computational Cost Nonlinear Formulation for Multibody Railroad Vehicle Systems. *2007 Proceedings of the ASME International Design Engineering Technical Conferences and Computers and Information in Engineering Conference, DETC2007*, Vol. 5 PART C, 2009, pp. 1847–1856. https://doi.org/10.1115/DETC2007-34522.
19. Wu, Q., C. Cole, S. Luo, and M. Spiryagin. A Review of Dynamics Modelling of Friction Draft Gear. *Vehicle System Dynamics*, Vol. 52, No. 6, 2014, pp. 733–758. https://doi.org/10.1080/00423114.2014.894199.
20. Cipek, M., D. Pavković, Z. Kljaić, and T. J. Mlinarić. Assessment of Battery-Hybrid Diesel-Electric Locomotive Fuel Savings and Emission Reduction Potentials Based on a Realistic

Mountainous Rail Route. *Energy*, Vol. 173, 2019, pp. 1154–1171. https://doi.org/10.1016/j.energy.2019.02.144.
21. American Railway Engineering and Maintenance-of-Way Association. *AREMA Manual for Railway Engineering*. 2021.
22. Fadhloun, K., and H. Rakha. A Novel Vehicle Dynamics and Human Behavior Car-Following Model: Model Development and Preliminary Testing. *International Journal of Transportation Science and Technology*, Vol. 9, No. 1, 2020, pp. 14–28. https://doi.org/10.1016/J.IJTST.2019.05.004.
23. Wang, J., and H. A. Rakha. Longitudinal Train Dynamics Model for a Rail Transit Simulation System. *Transportation Research Part C: Emerging Technologies*, Vol. 86, No. October 2017, 2018, pp. 111–123. https://doi.org/10.1016/j.trc.2017.10.011.
24. Hay, W. W. *Railroad Engineering*. John Wiley \& Sons, 1991.
25. Brandenburger, N., and M. Jipp. Effects of Expertise for Automatic Train Operations. *Cognition, Technology & Work*, Vol. 19, No. 4, 2017, pp. 699–709. https://doi.org/10.1007/s10111-017-0434-2.
26. Wang, J., and H. A. Rakha. Electric Train Energy Consumption Modeling. *Applied Energy*, Vol. 193, 2017, pp. 346–355. https://doi.org/10.1016/J.APENERGY.2017.02.058.
27. Dion, F., H. Rakha, and Y.-S. Kang. Comparison of Delay Estimates at Under-Saturated and over-Saturated Pre-Timed Signalized Intersections. *Transportation Research Part B: Methodological*, Vol. 38, No. 2, 2004, pp. 99–122.
28. Rakha, H., Y.-S. Kang, and F. Dion. Estimating Vehicle Stops at Undersaturated and Oversaturated Fixed-Time Signalized Intersections. *Transportation Research Record*, Vol. 1776, No. 1, 2001, pp. 128–137.
29. Wang, J., A. Ghanem, H. Rakha, and J. Du. A Rail Transit Simulation System for Multi-Modal Energy-Efficient Routing Applications. *International Journal of Sustainable Transportation*, Vol. 15, No. 3, 2021, pp. 187–202. https://doi.org/10.1080/15568318.2020.1718809.